ARMY RESEARCH LABORATORY

Reconstruction of Aerosol Properties from Forward-scattering Intensities

by Dr. Gorden Videen and Dr. Matthew Berg

ARL-MR-0763 **January 2011**

NOTICES

Disclaimers

The findings in this report are not to be construed as an official Department of the Army position unless so designated by other authorized documents.

Citation of manufacturer's or trade names does not constitute an official endorsement or approval of the use thereof.

Destroy this report when it is no longer needed. Do not return it to the originator.

Army Research Laboratory
Adelphi, MD 20783-1197

ARL-MR-0763 **January 2011**

Reconstruction of Aerosol Properties from Forward-scattering Intensities

Dr. Gorden Videen and Dr. Matthew Berg
Computational and Information Sciences Directorate, ARL

REPORT DOCUMENTATION PAGE

Form Approved
OMB No. 0704-0188

1. REPORT DATE *(DD-MM-YYYY)*	2. REPORT TYPE	3. DATES COVERED (From - To)
January 2011	DRI	FY10

4. TITLE AND SUBTITLE
Reconstruction of Aerosol Properties from Forward-scattering Intensities

5a. CONTRACT NUMBER

5b. GRANT NUMBER

5c. PROGRAM ELEMENT NUMBER

6. AUTHOR(S)
Dr. Gorden Videen and Dr. Matthew Berg

5d. PROJECT NUMBER

5e. TASK NUMBER

5f. WORK UNIT NUMBER

7. PERFORMING ORGANIZATION NAME(S) AND ADDRESS(ES)
U.S. Army Research Laboratory
ATTN: RDRL-CIE-S
2800 Powder Mill Road
Adelphi, MD 20783-1197

8. PERFORMING ORGANIZATION REPORT NUMBER
ARL-MR-0763

9. SPONSORING/MONITORING AGENCY NAME(S) AND ADDRESS(ES)

10. SPONSOR/MONITOR'S ACRONYM(S)

11. SPONSOR/MONITOR'S REPORT NUMBER(S)

12. DISTRIBUTION/AVAILABILITY STATEMENT
Approved for public release; distribution unlimited.

13. SUPPLEMENTARY NOTES

14. ABSTRACT
This work describes the design and application of an apparatus to image aerosol particles using digital holography in a flow-through, contact-free manner. Particles in an aerosol stream are illuminated by a triggered, pulsed laser and the pattern produced by the interference of this light with that scattered by the particles is recorded by a digital camera. The recorded pattern constitutes a digital hologram from which an image of the particles is computationally reconstructed using a fast Fourier transform. This imaging is validated using a cluster of ragweed pollen particles. Examples involving mineral-dust aerosols demonstrate the technique's in situ imaging capability for complex-shaped particles over a size range of roughly 15–500 μm. The focusing-like character of the reconstruction process is demonstrated using a sodium chloride (NaCl) aerosol particle and is compared to a similar particle imaged with a conventional microscope.

15. SUBJECT TERMS
Aerosols, holography

16. SECURITY CLASSIFICATION OF:			17. LIMITATION OF ABSTRACT	18. NUMBER OF PAGES	19a. NAME OF RESPONSIBLE PERSON
a. REPORT	b. ABSTRACT	c. THIS PAGE			Gorden Videen
Unclassified	Unclassified	Unclassified	UU	24	19b. TELEPHONE NUMBER (*Include area code*) (301) 394-1871

Standard Form 298 (Rev. 8/98)
Prescribed by ANSI Std. Z39.18

Contents

List of Figures

Acknowledgments

We are thankful for multiple helpful discussions with Yong-Le Pan, Steve Hill, Dave Ligon, Chris Sorensen, and Jay Eversole.

INTENTIONALLY LEFT BLANK.

1. Objective

The objective of this research is to explore, develop, and demonstrate the feasibility of using the two-dimensional angular optical scattering (TAOS) forward-scattering signals to reconstruct profiles of aerosol particles, providing information that can be used to characterize them and identify potential threats.

2. Approach

The in situ characterization of small particles is a persistent objective in applied physics and engineering contexts. Examples include the determination of atmospheric aerosol compositions for climate modeling and the detection of biological weapons agents for defense applications. Countless measurements and calculations of single- and multiple-particle scattering patterns can be found in the literature. The overall goal of such work is to infer information relating to the particles' physical form, such as size and shape, by analyzing the angular structure of these patterns (*1*). Unfortunately, a fundamental limitation of this approach is the absence of an unambiguous quantitative relationship between a pattern and the corresponding particle's properties, i.e., the so-called "inverse problem." Consequently, the inference of these properties from the patterns has proved to be very difficult in practice, except for the simplest of cases.

Ideally, one would prefer to image the particles directly, thus eliminating the complexity and ambiguity associated with interpretation of the scattering patterns. However, the typical particle size range of interest for many applications is roughly 0.1 to 10 μm (*1, 2*). Because of this, direct images are possible only with high numerical-aperture (NA) optics and correspondingly small focal volumes. This typically requires collection and immobilization of particle samples, and thus, such imaging is not a practical technique for particle characterization in applications requiring high sample throughput or images of the particles in their undisturbed form, i.e., in situ images.

Holography is an alternative technique that combines useful elements of both conventional imaging and scattering. Fundamentally, this is a two-step process. First, an object is illuminated with coherent light and the intensity pattern resulting from the interference of this light with that scattered by the particle is recorded. This pattern constitutes the hologram, from which an image of the object is reconstructed. Traditionally, holograms are recorded with photographic film due to the film's high resolution, which is required to capture the finer features of the interference pattern. The subsequent chemical development of the film is costly and time consuming, and this greatly limits the practical utility of the technique. For this reason, charge-coupled device (CCD) detectors are used to record the interference pattern. The resulting so-called digital

hologram can then be computationally processed, rather than chemically, to reconstruct an image of the object.

Digital holographic imaging has been demonstrated in multiple small-particle systems, see references 3–9, for example. Examples of work applying holography to aerosols are scarce and, to the best of our knowledge, this area has not yet been reported for in situ imaging of aerosol particles in the 0.1–25 μm size range. This report describes the design and implementation of an apparatus that achieves imaging of particles approximately 15–500 μm in size and has the potential to image particles as small as 4 microns given further design optimization. The basic concepts involved are briefly reviewed and a validation measurement using ragweed pollen particles is presented. Saharan, Tunisian, and sodium chloride (NaCl) aerosols are used to establish the capability of the apparatus. Finally, the microscope-like focusing behavior of the image-reconstruction process is demonstrated using a single NaCl aerosol particle.

The apparatus in this work is based on the so-called in-line holographic configuration (*3*). Here, the particle, primary optical components, and detector are all co-linearly arranged. The particle is illuminated by a monochromatic spherical wave and the resulting interference pattern formed by this reference wave and the light scattered by the particle is recorded by a CCD detector. Let the source of the reference wave be located a distance *l* from the particle and the detector at a distance *d* from the particle. Provided that *kl* and *kd* are large enough to satisfy the far-field conditions of (*10*), both the reference and scattered waves will be transverse and spherical at the detector and can be represented entirely by their scattering amplitudes

$$E^{ref}(r) = \frac{e^{ikr}}{r} E_1^{ref}(\hat{r}), \quad E^{sca}(r) = \frac{e^{ikr}}{r} E_1^{sca}(\hat{r}), \tag{1}$$

respectively. Then, the intensity of the total wave across the detector's face is (*3*)

$$\begin{aligned} I^{holo}(r) &= |E_1^{ref}(\hat{r}) + E_1^{sca}(\hat{r})|^2 \\ &= |E_1^{ref}(\hat{r})|^2 + |E_1^{sca}(\hat{r})|^2 + [E_1^{ref}(\hat{r})]^* E_1^{sca}(\hat{r}) + [E_1^{sca}(\hat{r})]^* E_1^{ref}(\hat{r}). \end{aligned} \tag{2}$$

The quantity $|E_1^{ref}(\hat{r})|^2 = I^{ref}(r)$ in equation 2 is the intensity across the detector when no particle is present, and hence, can be considered a known quantity measured before the introduction of an aerosol sample. Subtracting this reference intensity from equation 2 and dividing the remaining terms by it gives

$$\begin{aligned} I^{con}(r) &= \frac{I^{holo}(r) - I^{ref}(r)}{I^{ref}(r)} \\ &= \frac{|E_1^{sca}(\hat{r})|^2}{I^{ref}(r)} + \frac{[E_1^{ref}(\hat{r})]^* E_1^{sca}(\hat{r}) + [E_1^{sca}(\hat{r})]^* E_1^{ref}(\hat{r})}{I^{ref}(r)}. \end{aligned} \tag{3}$$

Often, the intensity of the reference wave at the detector is much greater than that of the scattered wave. This is especially true in this work where the objects being illuminated are small particles, as opposed to the macroscopic-sized objects involved in other work (*11–14*). This means that the term $|E_1^{sca}(\hat{r})|^2/I^{ref}(r)$ in equation 3 can be neglected, leaving

$$I^{con}(r) = \frac{[E_1^{ref}(\hat{r})]^* E_1^{sca}(\hat{r}) + [E_1^{sca}(\hat{r})]^* E_1^{ref}(\hat{r})}{I^{ref}(r)}. \quad (4)$$

This intensity pattern, which is the difference between two measurements (with and without the particle present), is known as a contrast hologram. The key characteristic of I^{con} is its linear dependence on the amplitude of the particle's scattered wave. This means that the phase of the wave over the detector is encoded in the measurement. Consequently, I^{con} can be used to reconstruct unambiguously an image of the particle that closely resembles that obtained from conventional microscopy.

Because there are many references describing the theory behind digital holographic imaging, only a brief description is given here (*15, 16*). The contrast hologram is envisioned as a transmission diffraction grating illuminated by a normally incident plane wave, i.e., a reconstruction wave. The Fresnel-Kirchhoff approximation is then used to describe the light diffracted from this grating in a parallel plane separated by a distance *z* from the grating along the *z*-axis. If *z* corresponds to the distance between the particle and detector during the hologram measurement ($z = d$), the resulting diffraction pattern in this so-called reconstruction plane yields an image of the particle. The image is essentially equivalent to a conventional microscope image, although the resolution may be less than the microscope image depending on the particle size (*3*).

The advantage of using the Fresnel-Kirchhoff approximation to calculate the reconstructed particle-image is that approximation's mathematical form is essentially a discrete Fourier transform of the CCD pixel values constituting I^{con}. This enables the use of the fast Fourier transform (FFT) in the calculation, thus substantially reducing the computation time required to render the particle image. This is fortuitous because in practice, *d* is not known to a great enough accuracy to be able to reconstruct an image from a single application of the reconstruction routine. This inaccuracy is due to the variation in particle positions in the aerosol stream as they enter the measurement volume. Consequently, the image reconstruction stage consists of a focusing-like procedure. First, an initial image is reconstructed using an estimate of *d* based on the experimental layout. Then, the reconstruction plane is scanned along the *z*-axis in small steps until the reconstructed image comes into focus. The ability to use the FFT for each of these intermediate steps is thus crucial to the practical implementation of this technique.

The primary drawback to the in-line configuration is that two images of the particle are produced in the reconstruction stage. The in-focus particle image is always accompanied by a blurred twin image that is in-focus in the mirror reconstruction-plane, i.e., at $z = -d$. As a consequence, the image quality is degraded. However, as shown in reference 3, the effect of the twin on the in-

focus image becomes negligible if both *d* and the size of the CCD pixel array are sufficiently large such that an imaging resolution on the order of the wavelength can be achieved (*3*, *4*).

Another drawback of in-line holography is the presence of the zero frequency, or so-called DC, term in the reconstructed image (*17*). In the diffraction grating model used to calculate the particle image, the reconstruction wave is uniform across the hologram since it is planar and normally incident. Upon application of the FFT to I^{con}, this wave then becomes a strong DC contribution in the transform. The result is an unwanted bright spot in the reconstructed image located at the intersection of the optical axis (*z*-axis) with the reconstruction plane. Fortunately however, the DC term can be nearly eliminated by subtracting from each pixel value in I^{con} the average value of all the pixels. Notice that in doing this subtraction, the result is a new contrast hologram with both positive and negative values; whereas, its constituent holograms I^{holo}, I^{ref}, and I^{con} are all inherently positive since they correspond to intensity measurements.

The resolution of the resulting particle images is limited by several factors related to diffraction and the apparatus hardware (*4*): the CCD pixel size Δx, CCD pixel-array size *w*, particle-CCD distance *d*, and the illumination wavelength λ. In short, the minimum resolvable length scale δ is approximately (*4*)

$$\delta = \frac{\lambda}{w}\sqrt{\left(\frac{w}{2}\right)^2 + d^2}\,. \tag{5}$$

For example, given the parameters of the apparatus in this work, which are described below, the theoretical maximum resolution is approximately 4 μm. However, the resolution achieved in practice is in the range of 8–10 μm due to stray-light noise and imperfections in the optical design. Note that $\sin\theta = (w/2)\sqrt{(w/2)^2 + d^2}$ from equation 5 is the NA of the arrangement as defined between the particle and detector, where θ is the angle subtended by the CCD array half-width. Thus, the resolution of this holographic configuration will not exceed what is possible from a conventional optical microscope. However, as discussed earlier, it does provide the substantial advantage of near real-time, in situ, and high throughput imaging, which is not possible with conventional microscopy.

3. Results

The experimental apparatus shown in figure 1 consists of two primary subsystems: aerosol-particle sensing and hologram recording. An aerosol stream is delivered via a nozzle made from a plastic pipettor tip to the measurement volume where an optical trigger is used to sense the presence of a particle (*18*). This trigger consists of crossed diode laser beams, labeled (h) and (i) in figure 1. These lasers have different wavelengths of 635 and 670 nm and intersect near the outlet nozzle delivering the aerosol. When a particle passes into this intersection, it scatters both wavelengths of light simultaneously. The scattered light is received by two photomultiplier

(PMT) modules (Hamamatsu Corp., model H6780-02), each sensitive to only one of the two wavelengths. A series of signal analysis units determines if the signals produced by the PMT modules are coincident. If so, this indicates the presence of a particle at the trigger laser beam intersection and a fire signal is sent to a pulsed laser for the hologram recording.

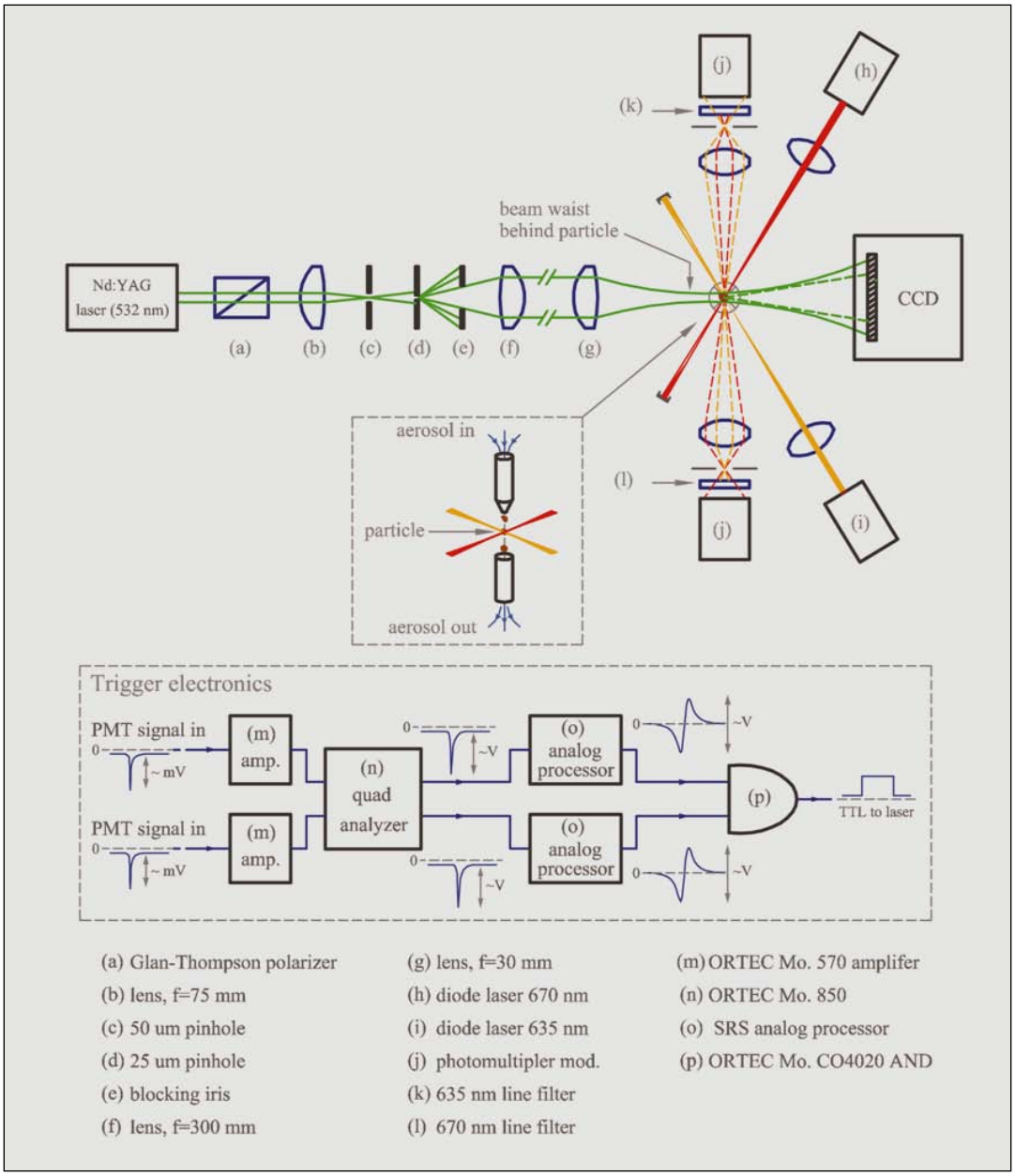

Figure 1. Diagram of the digital holographic imaging apparatus. The middle inset shows a schematic of the signal analysis used in the optical trigger to sense the presence of a particle in the measurement volume. See text for further explanation.

The triggered light source is a 70-ns pulsed neodymium (Nd): yttrium aluminum garnet (YAG) laser (Spectra Physics Lasers, Inc., model Y70-532Q), frequency doubled to 532 nm. This light

passes through a Glan-Thompson polarizer to ensure linear polarization, (a) in figure 1. The light is then focused by lens (b) onto a 50-μm-diameter pinhole (c). Next, an iris (d) is used to block all but the primary lobe of this pinhole diffraction pattern from reaching a second pinhole (e) with a diameter of 25 μm. These pinholes "clean" the beam, improving its spatial coherence and enhancing the quality of the hologram. Following this, the lens (f) collimates the beam, which is then brought to a focus by another lens (g) at a point approximately 2 mm from the aerosol nozzle outlet. This 2 mm is distance *l*. In this way, the aerosol particles are illuminated by what is approximately a spherical wave originating from the beam waist. The beam continues until reaching the CCD detector, at which point it expands to fill the entire pixel array. The separation between the particle stream and the detector is the distance *d*, discussed previously, and is approximately 8 cm. A small amount of the beam is scattered by the particle that activated the optical trigger, and this scattered light interferes with the remainder of the beam, i.e., the reference wave, to form the interference pattern that becomes the digital hologram I^{holo}.

To test the apparatus and calibrate the previously outlined image reconstruction procedure, a comparison is made between a holographic and optical microscope image of the *same* particle. This is done by placing 15.4-μm-diameter National Institute of Standards & Technology (NIST)-traceable polystyrene latex microspheres (Duke Scientific Corp.) on a microscope slide and positioning the slide in the measurement volume at the intersection of the trigger-beams. A hologram is recorded, on which the image reconstruction procedure is followed. The slide is then transferred to a microscope, where the same spheres are located and imaged. Next, using a 1951 U.S. Air Force (USAF) glass slide resolution target (Edmund Optics), a scale factor is determined relating the microscope-image pixel number to micrometers. Then, by comparing the holographic image of a microsphere to the microscope image of the *same* microsphere, an additional scale factor is determined relating the hologram pixel number to micrometers. In this way, the holographic images of all subsequent particles can be rendered in calibrated length (micrometers), rather than pixel number.

An example is presented in figure 2 demonstrating the comparison between the holographic and microscope images of the same particle. Here a cluster of ragweed pollen particles is placed on a microscope slide, then holographic and microscope images of the cluster are obtained. By comparing these images, one can see that the holographic apparatus successfully produces an accurate image of the pollen cluster, with sufficient resolution to discern individual pollen particles and even a faint signature of the single-particle surface roughness seen in the microscope images. This corresponds to a resolution roughly between 8–10 μm, although a more rigorous resolution analysis is not performed. Referring to the measured and contrast holograms shown in this figure, one can see how subtraction of the incident beam across the CCD, i.e., I^{ref}, removes noise due to imperfections in the incident beam profile. This has the consequence of producing a "cleaner" contrast hologram, which subsequently improves the particle image.

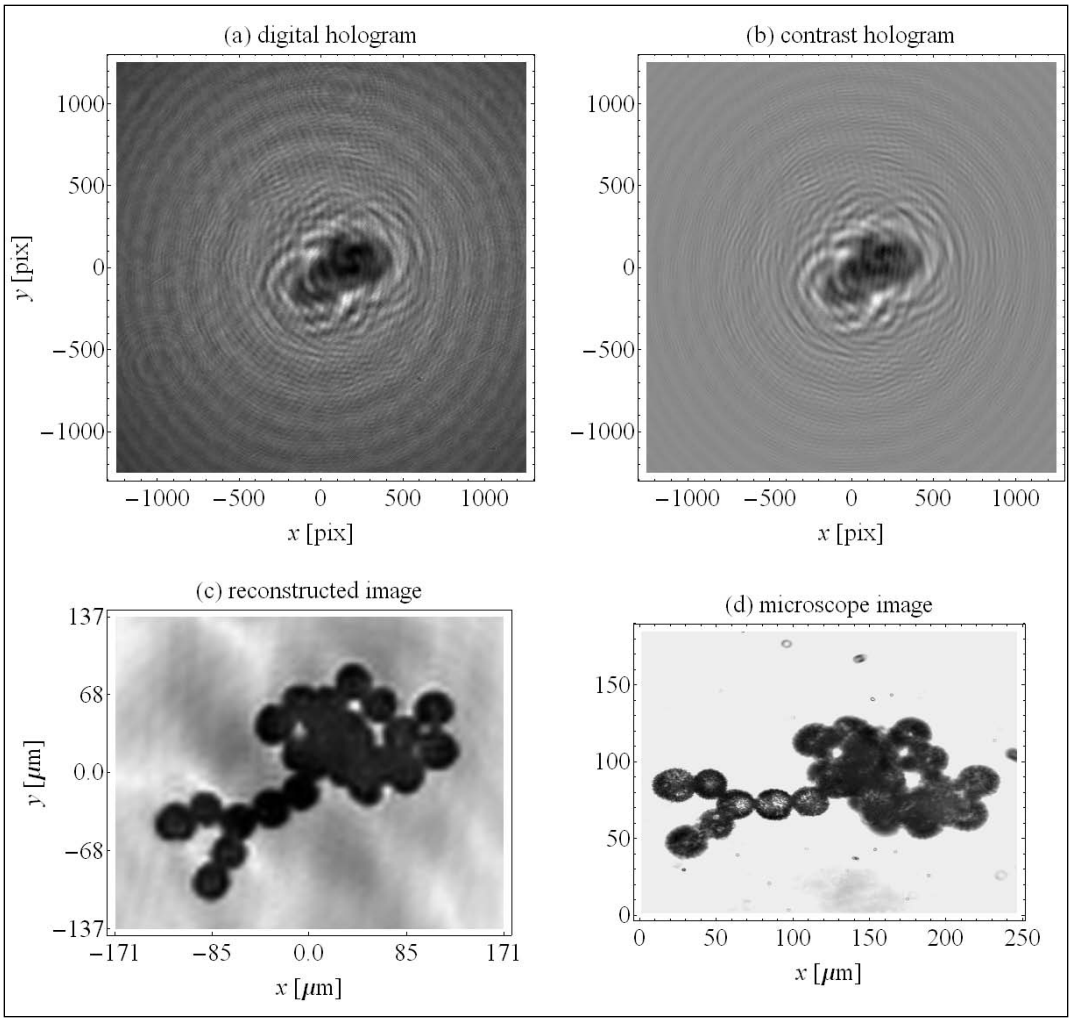

Figure 2. Validation of the holographic imaging apparatus. Plots (a) and (b) show the measured I^{holo} and corresponding contrast I^{con} holograms, respectively, for a cluster of ragweed pollen particles on a microscope slide located at the intersection of the trigger beams (recall figure 1). Image (c) shows the reconstructed image resulting from (b); whereas, (d) shows a conventional microscope image of the *same* cluster.

There are several unique aspects to the design of this apparatus. By using the short focal length lens (g) in figure 1 to form a beam waist near the particle, the light illuminating the particle is more intense than it would be if only the pinhole was used for illumination (as is usually done). This results in a relative amplification of the scattered wave at the detector and enhances the interference structure of the hologram leading to improved particle image quality. Using a pulsed laser permits the investigation of particle systems in motion. This also greatly relaxes the strict mechanical stability demands typically required for holographic measurements. There are no optical elements between the aerosol stream and the CCD camera. This gives the apparatus a working distance of several centimeters, which is substantially greater than the single- to sub-millimeter working distance of the microscope objective in conventional microscopy. Moreover, the absence of any optical element eliminates "noise" that can result from ambient dust that can collect on the optical surfaces.

To further assess the imaging capabilities of the apparatus, several aerosols consisting of complex-shaped particles are examined. The first samples are sieved Saharan and Tunisian sand, which are aerosolized using an Erlenmeyer flask as follows. A small sample of the sand is placed in the flask then sealed with a stopper. Two aluminum tubes pass through the stopper; one supplies air to the flask, blowing the sand particles around, while the other tube allows some of the airborne particles to exit the flask and be transported to the aerosol nozzle in the apparatus. Figure 3 shows the contrast holograms along with the resulting particle image reconstructions for single Saharan and Tunisian sand particles. For comparison, figure 4 shows conventional optical microscope images of these sand samples. One can see that the holographic images provide the same information of overall particle size and morphology as the microscope images. For example, the Saharan particles appear to have less surface roughness than the Tunisian particles.

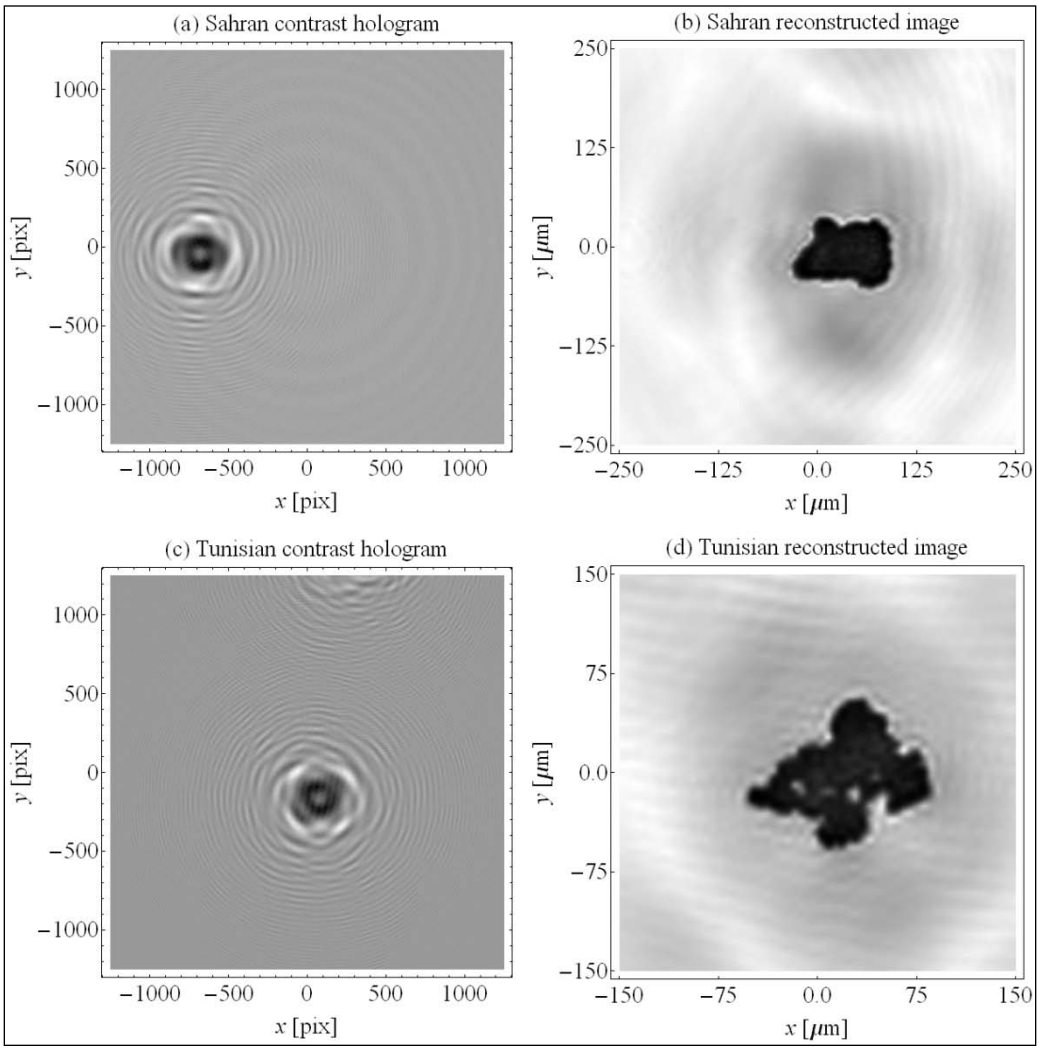

Figure 3. Saharan and Tunisian sand particles. Images (a) and (b) show the contrast hologram and corresponding reconstructed image for a single Saharan sand particle, and images (c) and (d) show the same for a single Tunisian sand particle.

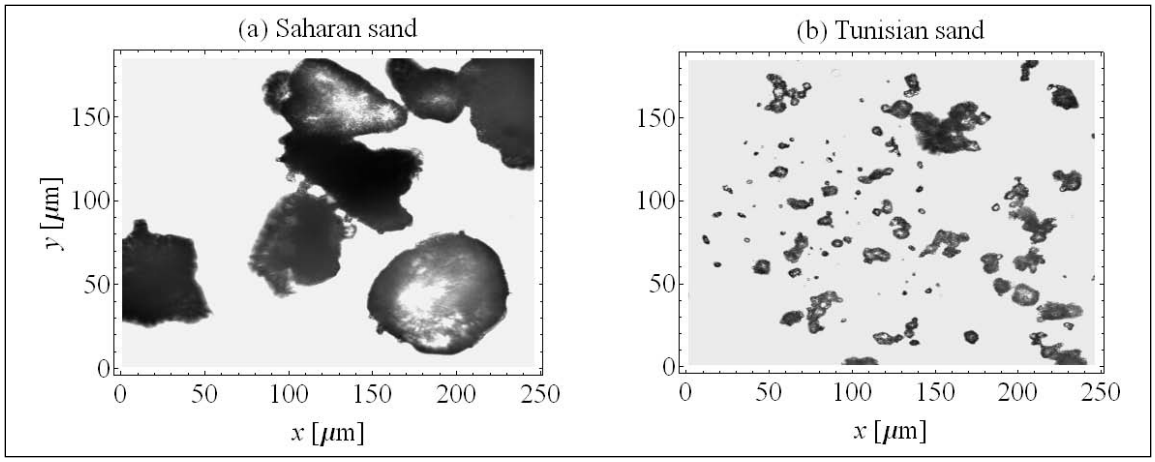

Figure 4. Microscope images of Saharan and Tunisian sand. The particles seen here are taken from the same sand samples used in figure 3, but unlike the ragweed in figure 2, these particles are not the exact same particles imaged holographically.

Another unique capability of holographic imaging is that some sense of the three-dimensional form of a particle can be garnered from a *single* measurement. The basic idea is analogous to the "focusing in" on a particle in conventional microscopy. There, the microscope objective is moved vertically to vary the distance between it and the microscope slide, causing a blurred image of a particle to evolve into a sharp image. If the particle has sufficient thickness and transparence, different depths within the particle can be brought into focus to give a feel for the particle's three-dimensional structure. This same process can be done in digital holography by computationally varying the distance d used in the image reconstruction stage, as is shown by Xu et al. (*3*). The resulting sequence of images gives the same impression of focusing in on the particle as one gets from microscopy. However, unlike microscopy where an image must be recorded at each "focus depth," the holographic route can obtain a similar image sequence from the contrast hologram only.

Figure 5 shows an example of this holographic focusing process. The top row displays conventional microscope images of a NaCl crystal at different focus depths; whereas, the bottom row shows a holographic image sequence for an aerosolized NaCl particle that is produced by scanning the reconstruction plane along the z-axis around $z = d$. The particle in the holographic images is delivered to the apparatus in aerosol form by drying a salt solution on a hotplate and aerosolizing the resulting powder using the Erlenmeyer generator described previously. One can clearly see the strong similarity in the focusing behavior of the two imaging techniques.

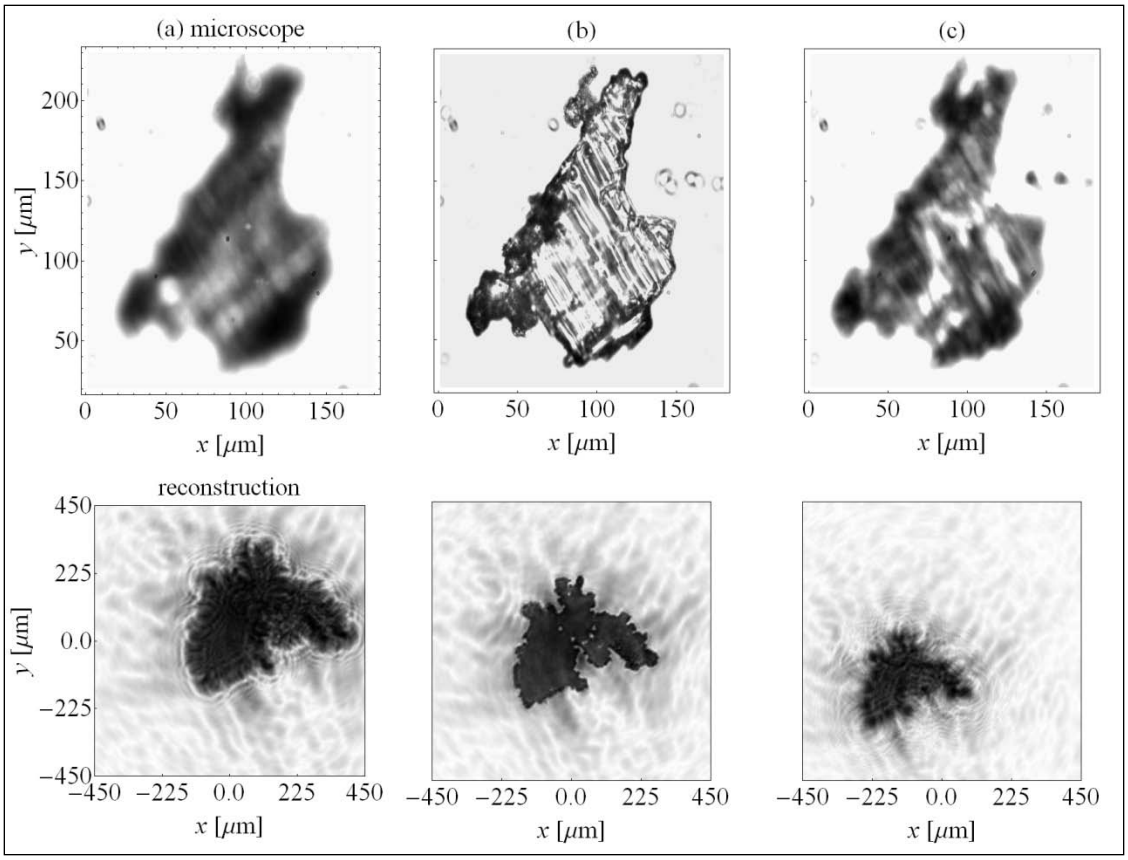

Figure 5. Focusing behavior of the holographic image-reconstruction process. The top row shows microscope images of a NaCl crystal at three different focus depths (a)–(c). The bottom row shows the reconstructed images of a NaCl aerosol particle when the reconstruction plane is at the three positions for z: $z < d$ for (a), $z = d$ for (b), i.e., in focus, and $z > d$ for (c).

The in-situ images of aerosol particles presented here are not the only documented examples. Sorensen et al. (*19*) have obtained images of the particles constituting hydrocarbon flame soot at various stages in soot formation, i.e., as a function of height in a flame. Here a 10× power photomicroscope is mated to a conventional film-camera and a 1.5-μs xenon (Xe) flash lamp is used for particle illumination. With this arrangement, particles in the range of roughly 5–100 μm are imaged, which covers the same particle size range considered in our work. One might then wonder what advantage the holographic approach offers over this photomicroscope direct imaging.

First, our holograms are entirely digitally recorded and the resulting images are computationally rendered. Second, and perhaps most important, the photomicroscope images have a very narrow depth of field, and only particles constrained within a narrow volume are in focus; whereas, for holographic techniques the focusing is done computationally, after the hologram is recorded. This enables the computational focusing process described previously, which can be used to image multiple particles present at different locations in the measurement volume as demonstrated by Xu et al. (*3*). Moreover, this can be done from a *single* hologram recording. To

do this with the photomicroscope approach would require obtaining a series of exposures with the microscope objective positioned at different distances from the measurement volume. Even if the film camera is replaced by a CCD, this would still require recording multiple images at the various focus depths. Thus, if the particles are in motion, as they are in all flow-through configurations, this would prevent the imaging of multiple particles present *at a given instant* in the measurement volume.

As mentioned previously, an inherent advantage of the holographic design is that there are no optical elements between the particle and detector. Thus, there are no surfaces for ambient dust to collect on and become sources of stray light, nor are there any lens-based spherical aberrations and multiple reflections. Both of these concerns are present in the photomicroscope approach. The absence of these optical elements in the holographic design is especially advantageous when one wishes to investigate particles that are roughly the same size as ambient dust.

4. Conclusions

This work demonstrates the feasibility of imaging single and multiple aerosol particles in-situ using digital in-line holography. Imaging is demonstrated on ragweed pollen, Saharan and Tunisian sand, and NaCl particles, covering a range of overall particle-size of approximately 15–500 μm. These images are computationally reconstructed from the digitally recorded holograms and compare well in quality and accuracy to the corresponding microscope images. Although the resolution of the holographic images is less than those from the microscope, one is able to clearly discern the size and shape of a single particle. Moreover, the ability to computationally render the images allows the application of numerical operations to improve image quality, whereas the analogs of such operations in conventional optical imaging would be difficult to implement.

5. References

1. Aptowicz, K. B.; Pinnick, R. G.; Hill, S. C.; Pan, Y. L.; Chang, R. K. Optical Scattering Patterns from Single Urban Aerosol Particles at Adelphi, Maryland, USA: A Classification Relating to Particle Morphologies. *J. Geophys. Res.* **2006**, *111*, D12212.
2. Hoekstra, A.; Maltsev, V.; Videen, G. Eds., *Optics of Biological Particles*; Springer, Dordrecht, 2007.
3. Xu, W.; Jericho, M. H.; Meinertzhagen, I. A.; Kreuzer, H. J. Digital In-line Holography of Microspheres. *Appl. Opt.* **2002**, *41*, 5367–75.
4. Garcia-Sucerquia, J.; Xu, W.; Jericho, S. K.; Klages, P.; Jericho, M. H.; Kreuzer, H. J. Digital In-line Holographic Microscopy. *Appl. Opt.* **2006**, *45*, 836–50.
5. Kreuzer, H. J.; Jericho, M. J.; Meinertzhagen, I. A.; Xu, W. Digital In-line Holography with Photons and Electrons. *J. Phys.: Condens. Matter* **2001**, *13*, 10729–41.
6. Raupach, S.M.F.; Vossing, H. J.; Curtius, J.; Borrmann, S. Digital Crossed-beam Holography for *In-situ* Imaging of Atmospheric Ice Particles. *J. Opt. A: Pure Appl. Opt.* **2006**, *8*, 796–806.
7. Fugal, J. P.; Shaw, R. A. Cloud Particle Size Distributions Measured with an Airborne Digital In-line Holographic Instrument. *Atmos. Meas. Tech.* **2009**, *2*, 259–71.
8. Singh, V. R.; Hegde, G.; Asundi, A. Particle Field Imaging Using Digital In-line Holography. *Current Sci.* **2009**, *96*, 391–97.
9. Thompson, B. J. Holographic Particle Sizing Techniques. *J. Phys. E: Sci. Instrum.* **1974**, *7*, 781–88.
10. Mishchenko, M. I.; Travis, L. D.; Lacis, A. A. *Multiple Scattering of Light by Particles: Radiative Transfer and Coherent Backscattering*; Cambridge University Press, Cambridge, 2006.
11. Schnars, U.; Juptner, W. Direct Recording of Holograms by a CCD Target and Numerical Reconstruction. *Appl. Opt.* **1994**, *33*, 179–81.
12. Zhang, S. Application of Super-resolution Image Reconstruction to Digital Holography. *EURASIP J. Appl. Signal Process. 2006, article ID 90358*, 1–7.
13. Ma, L.; Wang, H.; Li, Y.; Jin, H. Numerical Reconstruction of Digital Holograms for Three-dimensional Shape Measurement. *J. Opt. A: Pure Appl. Opt.* **2004**, *6*, 396–400.

14. Javidi, B.; Kim, D. Three-dimensional-object Recognition by Use of Single-exposure On-axis Digital Holography. *Opt. Lett.* **2005**, *30*, 236–38.

15. Kim, M. K. Principles and Techniques of Digital Holographic Microscopy. *SPIE Rev.* **2010**, *1*, 018005-1-50.

16. Ferraro, P.; De Nicola, S.; Coppola, G. Digital Holography: Recent Advancement and Prospective Improvements for Applications in Microscopy. in *Optical Imaging Sensors and Systems for Homeland Security Applications*, *Adv. Sci. Terch. Security Appl.* **2006**, *2*, 47–84.

17. Goodman, J. W. *Introduction to Fourier Optics*; Roberts & Company, Englewood (2005).

18. Pan, Y. L.; Holler, S.; Chang, R. K.; Hill, S. C.; Pinnick, R. G.; Niles, S.; Bottiger, J. R. Single-shot Fluorescence Spectra of Individual Micrometer-sized Bioaerosols Illuminated by a 351- or 266-nm Ultraviolet Laser. *Opt. Lett.* **1999**, *24*, 116–8.

19. Sorensen, C. M.; Hageman, W. B.; Rush, T. J.; Huang, H.; Oh, C. Aerogelation in a Flame Soot Aerosol. *Phys. Rev. Lett.* **1998**, *80*, 1782–85.

Sorensen, C. M.; Hageman, W. B. Two-dimensional Soot. *Langmuir* **2001**, *17*, 5431–34.

6. Transitions

This work currently is being written up for submission to the *Journal of Quantitative Spectroscopy and Radiative Transfer*. In addition, we are considering methods of analyzing aerosol images for characterization and the feasibility of incorporating such technology into aerosol detectors. The most pressing area of research to make this technology practical is the development of rapid algorithms to identify aerosols from image features.

List of Symbols, Abbreviations, and Acronyms

CCD	charge-coupled device
FFT	fast Fourier transform
NA	numerical-aperture
NaCl	sodium chloride
Nd	neodymium
NIST	National Institute of Standards & Technology
PMT	photomultiplier
TAOS	two-dimensional angular optical scattering
USAF	U.S. Air Force
Xe	xenon
YAG	yttrium aluminum garnet

No of. Copies	Organization
1 (PDF ONLY)	ADMNSTR DEFNS TECHL INFO CTR ATTN DTIC OCP 8725 JOHN J KINGMAN RD STE 0944 FT BELVOIR VA 22060-6218
1 HC	US ARMY RSRCH LAB ATTN RDRL CIM G T LANDFRIED BLDG 4600 ABERDEEN PROVING GROUND MD 21005-5066
3 HCS	US ARMY RSRCH LAB ATTN IMNE ALC HRR MAIL & RECORDS MGMT ATTN RDRL CIM L TECHL LIB ATTN RDRL CIM P TECHL PUB ADELPHI MD 20783-1197
1 HC	US ARMY RSRCH LAB ATTN RDRL CIE S G VIDEEN ADELPHI MD 20783-1197
2 HC	MISSISSIPPI STATE UNIVERSITY ATTN MATTHEW J BERG DEPARTMENT OF PHYSICS & ASTRONOMY MISSISSIPPI STATE MS 39762

TOTAL: 8 (1 ELEC, 7 HCS)